Polymer 231 (2021) 124116

Contents lists available at ScienceDirect

Polymer

journal homepage: www.elsevier.com/locate/polymer

Multi-layered polymerized high internal phase emulsions with controllable porosity and strong interfaces

Tucker J. McKenzie [a], Soren Smail [a], Kathryn Rost [a], Kabir Rishi [b], Gregory Beaucage [b], Neil Ayres [a,*]

[a] Department of Chemistry, The University of Cincinnati, P.O. Box 210172, Cincinnati, OH, 45221, USA
[b] Department of Chemical and Materials Engineering, The University of Cincinnati, Cincinnati, OH, 45242-0012, USA

ARTICLE INFO

Keywords:
PolyHIPE
Gradient porosity
Polydimethylsiloxane

ABSTRACT

Porous elastomers possessing gradient morphology or chemistry are needed for new applications including biomaterial interfaces, additive manufacturing, and separation membranes. However, elastomers possessing a porosity gradient are often difficult to prepare requiring slow multistep synthesis techniques. In this work, layered porosity polydimethylsiloxane (PDMS)-based polymerized high internal phase emulsions (polyHIPEs) with defined interfaces have been synthesized using one-step reactions. The total porosity, pore size, and surface area of the prepared polyHIPEs are controlled by varying the volume of aqueous dispersed phase in the emulsion. Analysis of SEM images and pore size calculations of layered porosity polyHIPEs proved the emulsion patterning method did not disrupt emulsion morphology and a clear porosity interface was maintained. Total porosity values dictate the storage moduli of the polyHIPEs, where highly porous materials possess the lowest observed moduli of ~70–90 kPa. Tensile testing shows that the interface between two layers is mechanically robust and does not split during elongation at break experiments. This work provides a simple technique to prepare layered porosity PDMS-based polyHIPEs having up to five tunable porosity layers with strong interfaces between the layers.

1. Introduction

Porous elastomers that possess structural or chemical properties in a spatially controlled manner are highly desirable for many applications including biomaterial interfaces [1–5] additive manufacturing [6,7], purification membranes [8], and acoustic manipulation as metamaterial wave guides [9,10]. For example, polymeric foams possessing a porosity gradient have been prepared for controlled wave front shaping in gradient-index acoustic materials [9]. These materials rely on controlling the porosity within distinct portions of the monolith. However, materials with a porosity gradient are often prepared using complex multistep synthesis techniques [11–15] or layer-by-layer approaches that may result in weak material interfaces [16].

One method to prepare highly-porous and gradient porosity materials is using an emulsion templating technique, or polymerized high internal phase emulsions (polyHIPEs) [17–23]. PolyHIPEs are defined by the amount of internal, or dispersed, phase stabilized within the continuous phase during emulsion preparation, and this dictates many of the material's properties [24,25]. The term *high* is defined as when the volume fraction of the dispersed-phase of the emulsion exceeds 74% of the total volume resulting in tightly packed droplets. Emulsions with 24–74% dispersed phase are called *medium* internal phase emulsions (MIPEs) while *low* internal phase emulsions (LIPEs) contain less than 24% of dispersed phase by volume [26]. Porous polymer monoliths are formed from the emulsion when a polymerizable continuous phase is cured followed by removal of the dispersed phase. Relatively few examples have been reported of polyHIPEs prepared with gradients in chemistry [27], porosity gradients [9,10,28–30], or a combination of both [28,31]. Layered porosity polyHIPEs (LP-polyHIPEs) have been prepared where either average pore size [29,31,32] or the total porosity is controlled [9,10]. Both approaches require spatial control over the final pore morphology. However, layered porosity polyHIPEs often require unique synthesis protocols such as microfluidics resulting in limited batch quantities [29,30].

The most widely reported polyHIPE synthesis technique is thermally initiated free radical polymerizations [33–35]. While free radical

* Corresponding author.
E-mail address: neil.ayres@uc.edu (N. Ayres).

https://doi.org/10.1016/j.polymer.2021.124116
Received 8 June 2021; Received in revised form 19 August 2021; Accepted 20 August 2021
Available online 25 August 2021

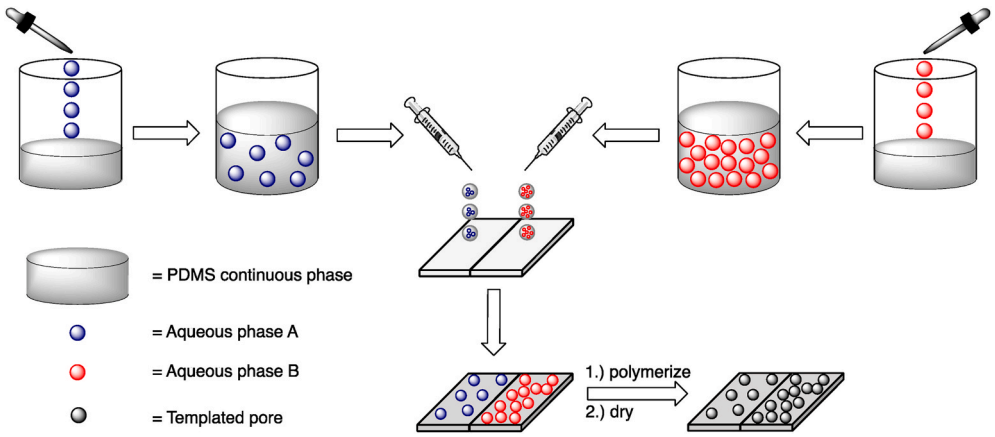

Fig. 1. Overview of layered polyHIPE synthesis by patterning two emulsions with different total volumes of dispersed phase. Emulsion formulation A **(blue)** can be patterned with emulsion formulation B **(red)** to produce a layered porosity polyHIPE after polymerization and drying. (For interpretation of the references to colour in this figure legend, the reader is referred to the Web version of this article.)

polymerizations are versatile and robust, a potential limitation of free radical polymerization is destabilization of the emulsions due to the elevated temperatures impacting emulsion stability or pore size causing undesirable final pore morphologies [36–38]. One alternative strategy is using orthogonal coupling reactions (or "click chemistry") [39,40] including thiol-ene reactions, typically with low molecular weight reactants [41–46]. Photoinitiated thiol-ene reactions can occur rapidly at room temperature to lock in droplet morphology [41]. Cameron and coworkers [31] demonstrated that rapid thiol-ene photopolymerizations of low-molecular weight monomers produced polyHIPEs with two layers by layering different emulsions together according to their composition, although the materials properties of the polyHIPEs were not tested. Well defined interfaces were produced that were attributed to limited inter-layer mixing due to the high viscosity inherent to HIPEs. In other work, Szabo and coworkers [47] patterned an elastomer consisting of hard and soft segments layered together. The patterned elastomers did not fracture at the interface between layers after curing, producing compositionally different layers with strong interfaces. Polydimethylsiloxane (PDMS) is often used as a non-porous elastomer, and porous PDMS materials have been prepared using polyHIPEs with both homogenous [48–51] and gradient [9,10] porosities using hydrosilylation or epoxy-curing reactions. Recently we reported that polyMIPEs can be prepared by reacting macromolecular thiol- and ene-functionalized PDMSs [51]. Building on our previous work with PDMS-based polyMIPEs, we investigated the ability to layer multiple emulsions together spanning MIPE to HIPE regimes, a currently unexplored topic. In the work reported here, we have prepared PDMS-based layered porosity polyHIPEs (LP-polyHIPEs) in a simple one-step process by patterning emulsions to form a single material using rapid thiol-ene click-chemistry reactions, as shown in Fig. 1. We have demonstrated that these reactions do not require any additional reagents or protocols compared to the monolithic polyHIPE synthesis.

We chose to cover a wide range in total porosity from 40% to 80% that spans both the MIPE and HIPE regimes, as both pore morphology and mechanical properties of the resulting polyHIPEs are impacted over this range. The volume of dispersed phase in the emulsion was found to dictate the average pore size and morphology as well as the mechanical properties after polymerization in a predictable fashion. Finally, the strength of the interface between two different formulations was tested by monitoring the break-point during tensile testing of the LP-polyHIPEs. While some of the materials prepared in this work are formally described as poly*MIPEs,* we are referring to all of the polymerized materials in this work as poly*HIPEs* for simplicity in naming and describing the layered materials. Furthermore, in the manuscript we identify the synthesized polyHIPEs according to their theoretical total porosity (Φ_{theo}) rather than their volume of dispersed phase in the emulsion templates.

2. Experimental

2.1. Materials

The photoinitiator 2,2-Dimethoxy-2-phenylacetophenone (DMPA) and reagent grade dichloromethane (DCM) were purchased from Sigma-Aldrich (St. Louis, MO, USA). The random copolymer [13–17% (mercaptopropyl) methylsiloxane]–dimethylsiloxane copolymer (thiolated-PDMS), the vinyl terminated polydimethylsiloxane (vinyl-PDMS), and (30–35% dodecylmethylsiloxane-[7–10% hydroxy(propethyleneoxy (6–9) propyl) methylsiloxane] – (55–65% dimethylsiloxane) terpolymer (Silube J208-812) were purchased from Gelest (Morrisville, PA, USA). Sodium Chloride (NaCl) was purchased from Oakwood Chemical (Estill, SC, USA). The blue dye used for imaging purposes, ORCOSOLVE Blue HF Liquid, was obtained from Orco Organic Dyes and Pigments (Lincoln, RI, USA). All reagents and chemicals were used as received without any modifications.

2.2. Methods

Total porosity calculations and density measurements were obtained from dried polyHIPE samples using a home-built Archimedes balance. Average pore morphology observations were obtained by analysis of scanning electron microscopy (SEM) images using a Scanning Electron Microscope (Low-Vac) (FEI XL-30) equipped with an EDAX detector. Cross sections of the materials were cut from dried polyHIPEs from chosen locations and fixed onto aluminum stubs, sputter coated with gold/palladium, and imaged at an accelerating voltage of 15 kV. Ultra small-angle X-ray scattering (USAXS) studies were carried out at beamline 9 ID-C at the Advanced Photon Source, at the Argonne National Laboratory [52–59]. Samples were prepared and scattering data was analyzed as described in our previous paper [51]. Viscoelastic properties of dried polyHIPEs were obtained using dynamic mechanical analysis (DMA) by a PerkinElmer Dynamic Mechanical Analyzer 8000 and processed using Pyris software. Sections of dried polyHIPEs were cut to ~3 mm thick, ~5 mm wide, and ~8 mm long. Each side of the interface and a sample of the interface between the two formulations were characterized for layered porosity materials (Fig. S1). Rectangular tension frequency sweep experiments (0.1–70 Hz; 0.01 mm strain) were run on three replicate samples for each polyHIPE formulation. The tensile strength-extension curves were recorded by an INSTRON 5948 Micro Tester equipped (Norwood, LA, USA) with a 5 N load cell.

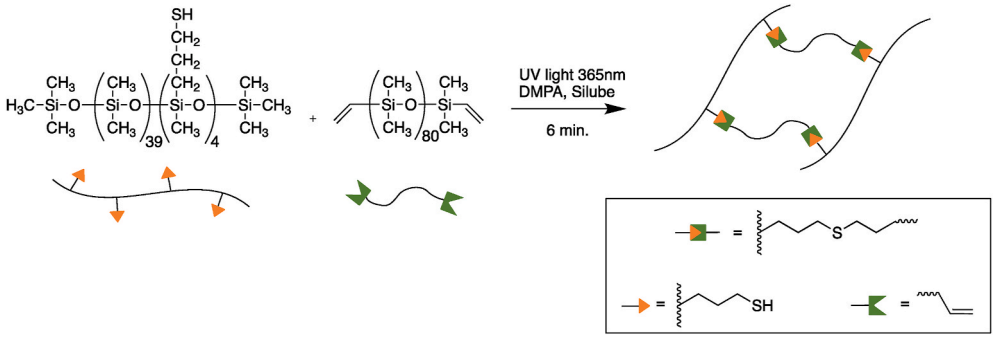

Scheme 1. Crosslinking reaction occurring in the continuous phase between thiolated-PDMS and vinyl-PDMS.

Triplicates for each sample were prepared in molds conforming to ASTM D412 – type C. These dog-bone specimens had an overall length of 115 mm (the gauge length being 25 mm), width of 6 mm, and thickness of 3 mm approximately. The sample thickness and width were measured three times, and the mean value was used for estimating the cross-sectional area. The samples were fixed to the test fixture on the INSTRON through pneumatic grips with automatically adjusting inlet air pressure. To prevent sample breakage while gripping, paper strips were placed between the sample and the serrated grips. All samples were strained at a crosshead speed of 5 mm/min or 0.2 inch/min during the tensile test. Constant tension was applied along the X-axis (Fig. S2) of the polyHIPEs to evaluate the strength at the interface of two formulations.

2.3. Emulsion preparation

Water-in-PDMS inverse emulsions were prepared using a protocol established in our lab [51]. A continuous phase containing equal thiol to alkene functional groups was prepared by adding thiolated-PDMS (2.5 g, 2.86 mmol thiol-functional groups) and vinyl-PDMS (8.57 g, 2.86 mmol alkene-functional groups) in a glass vial. Silube (111 mg) (1.0 wt % compared to total weight of continuous phase) was added and the mixture was vortexed for about 30 s to ensure a homogenous continuous phase was formed. A dispersed phase consisting of 1.5% wt/vol NaCl solution in ultra-pure Mili-Q water was added in about 1 mL portions to the vial containing the continuous phase to the desired volume of 40%–80%. After each addition of dispersed phase, the vial was vortexed for 2–3 min to form the emulsion until the required composition was obtained. Due to the increased viscosity, emulsions with >75% volume of dispersed phased needed to be prepared using an overhead stirrer with a propeller attachment at 800 rpm for 15 min following the same procedure. The size and morphology of dispersed phase droplets from each emulsion were characterized using optical microscopy (Fig. S3).

2.4. PolyHIPE synthesis

PolyHIPEs with a 1:1 ratio of thiol to alkene functional group were prepared using a modified procedure from our lab [51]. The continuous phase was first prepared in an appropriately-sized glass vial. Thiolated-PDMS (2.5 g, 2.86 mmol thiol-functional group), vinyl-PDMS (8.57 g, 2.86 mmol alkene-functional group), and Silube (111 mg, 1.0 wt % with respect to weight of continuous phase) were added and vortexed to mix. In a separate small glass vial the photoinitiator DMPA (111 mg, 1.0 wt% with respect to weight of continuous phase) was dissolved in approximately 0.2 mL of DCM. This solution was added to the continuous phase, vortexed until homogenous as previously described, and then protected from light. Nitrogen gas was bubbled through the reaction mixture to remove the DCM. The dispersed phase consisting of a 1.5% wt/vol NaCl solution in Mili-Q water was added in small portions and vortexed until a viscous emulsion formed. The emulsion was poured into the desired square or dog-bone shaped template and irradiated with UV light (λ_{max} = 365 nm, 48 W) for 6 min from all sides in a mirrored enclosure and allowed to stand further for 5 min before being removed and placed into the vacuum oven and dried for ~ 48 h at 24 °C. The polyHIPE was removed when a constant mass was obtained during the drying process. There was no further purification method performed after drying. The final polyHIPEs were characterized using scanning electron microscopy, USAXS, dynamic mechanical analysis and tensile testing in triplicate.

2.5. Layered porosity polyHIPE synthesis

Layered porosity polyHIPEs were prepared using a simple emulsion patterning method designed during this work. We first prepared polymerizable emulsions according to our methods where the volume of dispersed phase was varied from 40% to 80%. These emulsions were transferred into individual 12 mL syringes to more selectively fill the preferred portion of the template. Templates were previously 3D printed to have a slight notch along the inner wall to allow for a thin divider to be placed separating the two halves. One side of the template was filled with the first emulsion (A) and then a second emulsion (B) with a different formulation was used to fill the remaining half of the template (Fig. S4). The divider was slowly removed before placing the template immediately under the UV light source for 6 min. The layered polyHIPE was removed from the template and dried for ~48 h at 24 °C without any further purification. These materials were then cut into roughly three equally sized rectangular strips for dynamic mechanical analysis with a portion coming from only side A, only side B, and the interface of side A and B (Fig. S1). A dog bone-shaped template was used for preparing polyHIPEs for tensile testing where the same process of drying was followed without any additional cutting of the samples before characterization.

3. Results and discussion

We first prepared polyHIPEs using single-porosity emulsions with five different dispersed phase volume fractions spanning the MIPE and HIPE regimes from 40% to 80% volume of dispersed phase as controls for the LP-polyHIPEs. We varied the volume of the dispersed phase in these formulations as total porosity depends on the amount of dispersed phase and we hypothesized that the properties of these polyHIPEs are controlled through the total porosity. The aqueous dispersed phase of the emulsions was a 1.5 wt % salt solution of NaCl while the continuous phase consisted of UV-polymerizable pendent thiolated-PDMS and telechelic vinyl-PDMS with DMPA as the photoinitiator for the thiol-ene crosslinking reaction (Scheme 1).

The stoichiometric ratio of thiol to ene functional groups within the continuous phase was 1:1 and the concentration of both surfactant and photoinitiator were maintained at 1.0 wt % with respect to the continuous phase for all the formulations tested. We chose an equal thiol to ene ratio in this work as this ratio produced materials with the highest storage moduli in our previous study [51]. The droplet morphology in the emulsions were characterized before polymerization using optical

Table 1
Total porosity, pore size, and surface area results of single porosity **(SP-40 – SP-80)**.

PolyHIPE	Theoretical Total Porosity Φ_{theo} (%)	Total Porosity[a] Φ (%)	Average Pore Size[b] d_p (μm)	Average Surface Area[c] (m^2/g)
SP-40	40	40 ± 2	120 ± 0.4	0.035 ± 0.002
SP-60	60	58 ± 2	34 ± 0.1	0.261 ± 0.015
SP-70	70	62 ± 2	22 ± 0.1	0.457 ± 0.028
SP-75	75	53 ± 2	17 ± 0.1	0.416 ± 0.024
SP-80	80	3 ± 2	43 ± 0.1	0.004 ± 0.003

[a] Calculated from equation (1).
[b] Calculated from USAXS data.
[c] Calculated from equation (2).

microscopy (Fig. S3). All the emulsions showed similar aggregated droplets of dispersed phase where the diameter of the largest droplets was approximately 200 μm and the diameter of the smallest droplets was approximately 10 μm on average. These droplet-droplet interactions were expected, as emulsions stabilized by Silube surfactants have been reported to result in an aggregated droplets in water-in-PDMS emulsions [10,51].

We first characterized the single-porosity polyHIPEs with respect to their total porosity, pore size, and surface area, and these results are presented in Table 1.

We calculated the total porosity of the polyHIPEs using equation (1) where ρ is the average density of the bulk PDMS (0.975 g/mL), ρ^* is the measured density of individual polyHIPE samples (Table S1), and Φ is total porosity.

$$1 - \frac{\rho^*}{\rho} = \Phi \quad (1)$$

For polyHIPEs SP-40 and SP-60, a direct relationship exists where the volume of dispersed phase results in the expected total porosity. However, the values of total porosity are lower than expected for polyHIPEs SP-70 and SP-75. We explain this decrease in total porosity due to pore collapse during the drying process; this has been shown in similar soft PDMS-based porous monoliths [60]. The lowest calculated total porosity was polyHIPE SP-80, where the calculated total porosity of the material was negligible, and the measured density was also similar to that of non-porous crosslinked PDMS.

We calculated the average surface area (S_S) with Equation (2), using the average pore size, d_p, determined from USAXS data and the calculated porosity from equation (1).

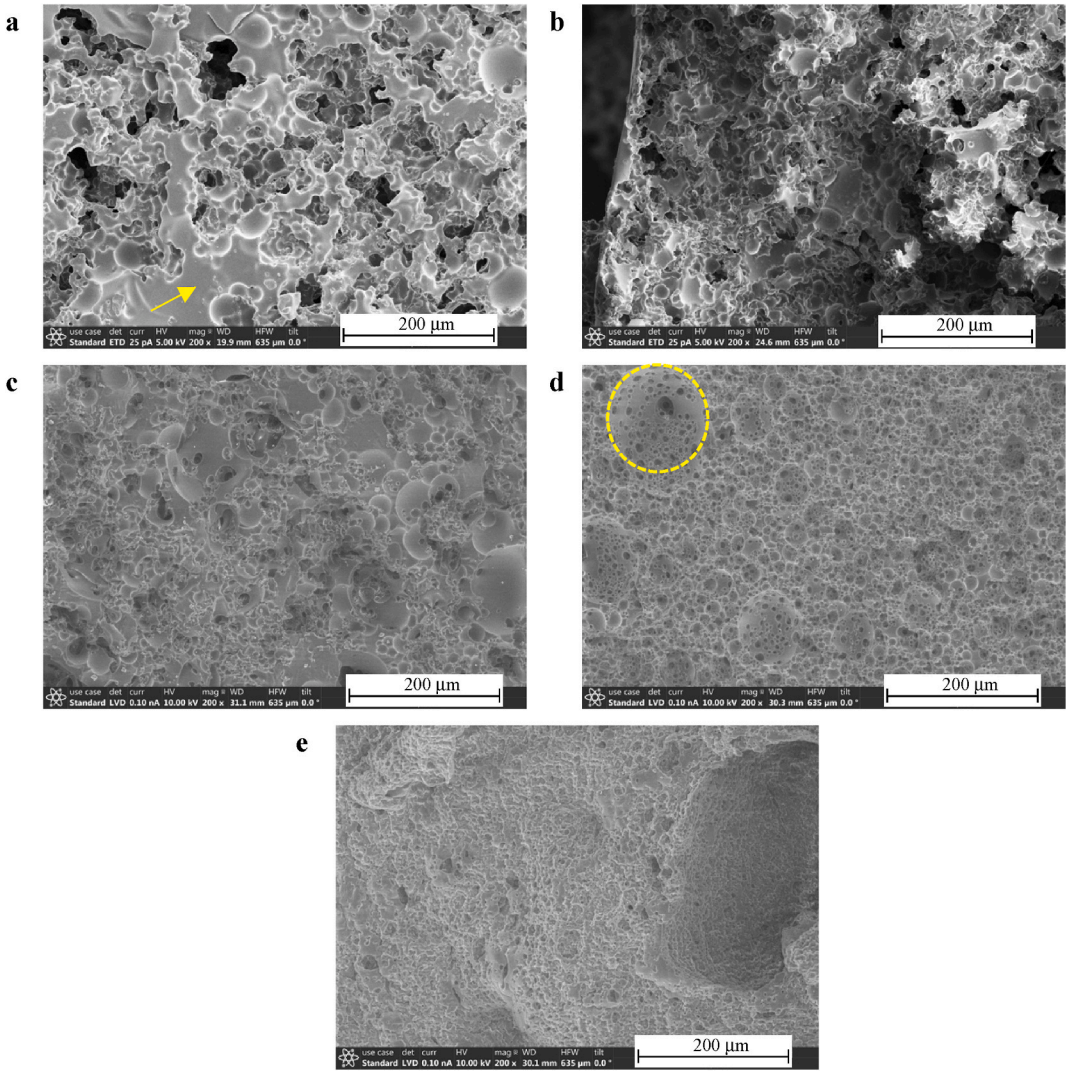

Fig. 2. SEM images of cross sections of dried polyHIPEs with varied single total porosity. **(a)** SP-40, **(b)** SP-60, **(c)** SP-70, **(d)** SP-75, and **(e)** SP-80. Areas of non-porous crosslinked PDMS are highlighted by a yellow arrow in image **(a)**. A yellow dashed circle in image **(d)** highlights pore window morphology. Scale bar is 200 μm for images. (For interpretation of the references to colour in this figure legend, the reader is referred to the Web version of this article.)

$$S_S = \frac{6\,\Phi}{(1-\Phi)\rho d_p} \sim 10^{-2} m^2/g \quad (2)$$

From the USAXS experiments, we observed a decrease in average pore size as Φ_{theo} increased. Specifically, polyHIPE SP-75 had the smallest average pore size at 17 μm while polyHIPE SP-40 had the largest at 120 μm. This was seen in all formulations besides polyHIPE SP-80 due to the significant pore collapse in those materials. As a result of the dramatic decrease in pore size, we see a corresponding increase in the surface area as we increased Φ_{theo}. For example, while polyHIPE SP-75 had the smallest average pore size, the surface area was slightly lower than polyHIPE SP-70 due to the lower total porosity. The pore collapse in polyHIPE SP-80 was further confirmed by our observation of the lowest surface area of 0.004 m^2/g for these materials. Our results from USAXS and porosity calculations of single porosity polyHIPEs established that significant changes to the pore size and total porosity were obtained over the range of dispersed phases tested. These results show that controlling pore size and total porosity can be achieved by simply changing the volume of dispersed phase of the emulsion in all cases besides emulsions consisting of 80% volume of dispersed phase for this system.

We further characterized single porosity polyHIPEs using SEM, and the images are shown in Fig. 2.

For all formulations, porous monoliths were obtained that had interconnected spherical pores with a dispersity in pore sizes. For polyHIPE SP-40 with a Φ_{theo} of 40% (Fig. 2a) an interconnected open-pore structure was obtained with areas of non-porous crosslinked PDMS, as highlighted by the yellow arrow in Fig. 2a. The observed interconnected structure support with the observations of the emulsions in optical microscopy, where aggregated water droplets surrounded by the PDMS continuous phase results in this observed open-pore structure. The non-porous area appears to decrease and a more homogenous spherical pore structure is formed as we increase Φ_{theo} to 60% and 70% in polyHIPE SP-60 and SP-70 respectively (Fig. 2b and c). When we increased the volume of dispersed phase into the polymerized *high* internal phase emulsion regime at a Φ_{theo} of 75% in polyHIPE SP-75 (Fig. 2d), we see an entirely interconnected open-pore morphology with no areas of non-porous PDMS. The appearance of pore throats between voids are observed on a more consistent basis across the entire monolith for this formulation highlighted with the dashed yellow circle in Fig. 2d. We do not see significant pore collapse in the SEM images for SP-70 and SP-75, even though we calculate lower total porosity values than expected from the formulation. We ascribe this to the method we used to measure the density of the polyHIPEs. Specifically, submerging the materials in water during the measurement can introduce error when calculating total porosity, as the interconnected porous structure of these highly porous materials makes them susceptible to infiltration of water when submerged. This causes a larger density to be measured resulting in the total porosity to be calculated incorrectly low. While we observed that the measured porosity in these materials was lower than the expected total porosity, and the discrepancy increases with the dispersed volume fraction, using the volume of the dispersed phase to control the total porosity of the polymerized material is an effective strategy when formulating the emulsion templates. As we further increased Φ_{theo} to 80% in polyHIPE SP-80, we see a complete loss of the spherical pore shape as well as pore windows and it resembled non-porous crosslinked PDMS. While the material largely becomes non-porous after calculations using density measurements, the SEM images showed a rough surface representative of residual collapsed pores.

Having obtained and characterized the SP-polyHIPEs to act as controlled comparisons, we then prepared the layered porosity polyHIPEs series by patterning two emulsions with different volumes of dispersed phases next to each other within a custom-built mold. We chose to hold one side of the material constant at a Φ_{theo} of 40% and for the remaining side, increased the Φ_{theo} from 60%, 70%, 75% and 80% to produce polyHIPEs with two distinct pore morphologies in a single material. The layered porosity polyHIPEs were subjected to the same porosity characterization as single porosity polyHIPEs and the results are detailed in Table 2.

We calculated the total porosity of the material at the interface between the two different formulations by taking a portion containing equal sizes of both sides and then performing density measurements. For example, the polyHIPE LP-40/60 was predicted to have a Φ_{theo} of 50% over the interface between emulsion templates. We found that this formulation possessed a total porosity of 48% falling between 40% and 60% as expected. We saw the same result in polyHIPEs LP-40/70 and LP-40/75 where the total porosity of the material at the interface was consistently between 40% and 70% or 40% and 75% respectively. PolyHIPE LP-40/80 possesses a dramatically decreased total porosity of 28%, which is again explained by the collapse of the 80% dispersed phase material. We performed USAXS experiments on each side of the interface (Table 2) for all the polyHIPEs and found that patterning two emulsions did not appear to disrupt the pore size or surface area of either side with respect to the single porosity control materials. We categorized the two sides of the LP-polyHIPEs as “Side A” and “Side B”. In every formulation the material from a 40% dispersed phase emulsion template is always Side A. The second portion of the LP-polyHIPE, Side B, is prepared from either polyHIPE SP-60, SP-70, SP-75, or SP-80 respectively. We observed similar trends for the surface area and pore size in the layered porosity materials compared to the single-emulsion templated materials, where pore size decreased when increasing the Φ_{theo} resulting in an increase in surface area. Interestingly, we also saw the side consisting of a Φ_{theo} of 75% in polyHIPE LP-40/75, obtained the highest surface area for all materials at 0.707 m^2/g. We hypothesize that in this case, the 40% porosity side of the interface could be acting as a support scaffold and limited the typical pore collapse found in this formulation allowing it to maintain a higher porosity, thus higher surface area. These results confirm that this emulsion patterning technique produced materials that maintained the expected pore morphology including pore size, shape, surface area, and overall total porosity in a controlled and spatially selective manner.

We characterized the pore morphology, size, and overall interface of LP-polyHIPEs using SEM, and the images are shown in Fig. 3.

Each LP-polyHIPE formulation produced materials with a defined interface highlighted with a yellow dashed line where two distinctly different pore morphologies in a single material are obtained

Table 2
Total porosity, pore size, and surface area results of layered porosity polyHIPEs **(LP-40/60 – LP-40/80)**.

PolyHIPE	Theoretical Total Porosity Φ_{theo} (%)	Total Porosity[a] Φ (%)	Average Pore Size[b] d_p (μm)		Average Surface Area[c] (m^2/g)	
	Interface		Side A	Side B	Side A	Side B
LP-40/60	50	48 ± 2	90 ± 0.3	41 ± 0.1	0.042 ± 0.003	0.217 ± 0.013
LP-40/70	55	49 ± 2	91 ± 0.3	18 ± 0.1	0.045 ± 0.003	0.530 ± 0.032
LP-40/75	57.5	46 ± 2	68 ± 0.2	12 ± 0.1	0.061 ± 0.004	0.707 ± 0.042
LP-40/80	60	28 ± 2	82 ± 0.3	35 ± 0.1	0.052 ± 0.003	0.259 ± 0.016

[a] Calculated from equation (1).
[b] Calculated from USAXS data.
[c] Calculated from equation (2).

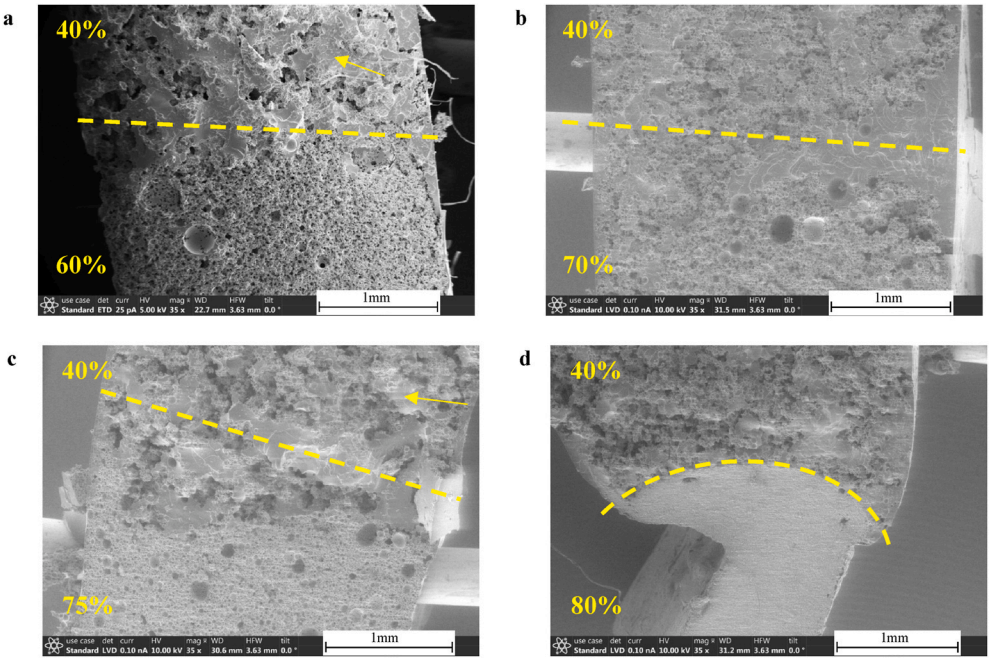

Fig. 3. SEM images of cross sections of dried polyHIPEs at the interface of layered porosity polyHIPEs. **(a)** LP-40/60, **(b)** LP-40/70, **(c)** LP-40/75, and **(d)** LP-40/80 where the interface between two different formulations is highlighted by a yellow dashed line in each image. The area above the dashed line is always Φ_{theo} of 40% in all images. Areas of non-porous crosslinked PDMS are highlighted by a yellow arrow in image **(a)** and **(c)**. Scale bar is 1 mm in each image. (For interpretation of the references to colour in this figure legend, the reader is referred to the Web version of this article.)

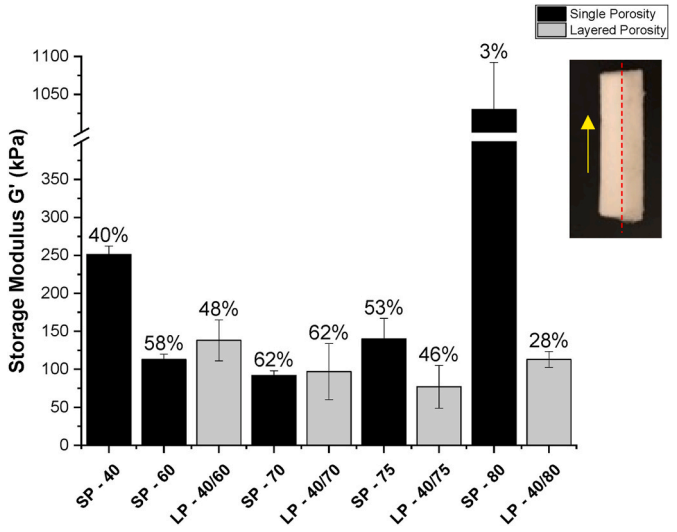

Fig. 4. Storage modulus at a single frequency plot of single porosity polyHIPEs (black columns) and the interface of layered porosity polyHIPEs (grey columns) where each are plotted as an average of three replicates. The calculated total porosity of each material is listed above individual bars. Inset image describes the direction of tension being applied (yellow arrow) to the interface (red dashed line) of layered porosity polyHIPEs. (For interpretation of the references to colour in this figure legend, the reader is referred to the Web version of this article.)

(Fig. 3a–d). We observed an interconnected open-pore structure with areas of non-porous crosslinked PDMS in the material comprised of a Φ_{theo} of 40% (top in Fig. 3a–d), as highlighted by the arrow in Fig. 3a. We observed differences comparing either side of the interface in these polyHIPEs, and the pore size and morphology change sharply at the interface. The non-porous areas appear to decrease, and a more homogenous spherical pore structure is formed on the side of the material with higher values of Φ_{theo} (bottom in images 3a-d). This difference in pore morphology is best observed in the layered materials with the largest differences between the porosity of the two formulations used to make the material. Overall, each layer in the LP-polyHIPE series is reflective of the SP formulation used to prepare the HIPE. For example, in PolyHIPE LP-40/75 (Fig. 3c) when each layer is compared to the corresponding single-porosity controls, i.e. SP-40 to Side A and SP-75 to Side B, we observe non-porous regions in Side A of the LP-polyHIPE where SP-40 had non-porous areas (**yellow arrow** in Fig. 3c) and SP-75 had entirely interconnected spherical pores similar to Side B of the LP-polyHIPE. We observe the expected loss of the spherical pore structure on the Φ_{theo} of 80% side in polyHIPE LP-40/80 (bottom Fig. 3d) due to pore collapse, and the interface became highly curved due to the collapse of the 80% side during the drying process while the Φ_{theo} of 40% porosity side of the material remained largely unaffected. This shrinkage of the 80% side due to pore collapse causes an entire slice of this material to bend (Fig. S5). Therefore, the collapse of the pore structure occurs independently of templating multiple emulsions together, and instead is a result of the formulation 80% itself. Collectively, SEM analysis of both layered and single porosity polyHIPE series, show that the process of templating two emulsions together does not disrupt the final pore structures but produces a single material with a defined interface.

Both series of polyHIPEs were characterized using DMA to obtain the storage moduli (G′) of the materials, and the results are detailed in Fig. 4. No variation in G′ was observed over the frequency range used so a single value at a frequency of 10 Hz is used in Fig. 4 for ease of comparison.

Mechanical analysis showed that the total porosity has an impact on the storage modulus, with SP-40 and SP-80 showing statistically significant different results from the other polyHIPEs. For the single-porosity polyHIPEs series, the materials with the highest porosity possess the lowest moduli. Specifically, PolyHIPE SP-70 had the lowest modulus at 92 kPa while having the highest total porosity of 62%. These results were expected as highly porous materials typically have lower mechanical properties [61,62]. The impact of pore collapse on the storage moduli of the polyHIPEs was observed for polyHIPEs SP-75 and SP-80. These materials were designed to have the highest total porosities and thus the softest materials, but we observed higher than predicted storage moduli of 140 kPa and 1030 kPa respectively due to the collapse of the interconnected pores. We performed the same analysis for the LP-polyHIPEs, where, as expected, the storage moduli showed no significant differences between the LP-polyHIPEs. For these measurements we recorded data using slices of the LP-polyHIPEs containing the interface, and applied the tension in the direction of the interface. The

Table 3
Mechanical analysis results of single porosity **(SP-40 – SP-80)** and layered porosity polyHIPEs **(LP-40/60 – LP-40/80)**. These results are from a single material rather than an average of replicates.

PolyHIPE	Total Porosity **Φ** (%)	Young's Moduli E (kPa)	Ultimate Tensile Strength σ_{ult} (kPa)	Fracture Strain ε_f (%)
SP-40	40	96	26	28
SP-60	59	70	60	81
SP-70	62	69	64	78
SP-75	52	74	57	77
SP-80	3	218	150	78
LP-40/60	49	87	43	48
LP-40/70	49	72	38	52
LP-40/75	47	92	50	54
LP-40/80	28	115	52	39

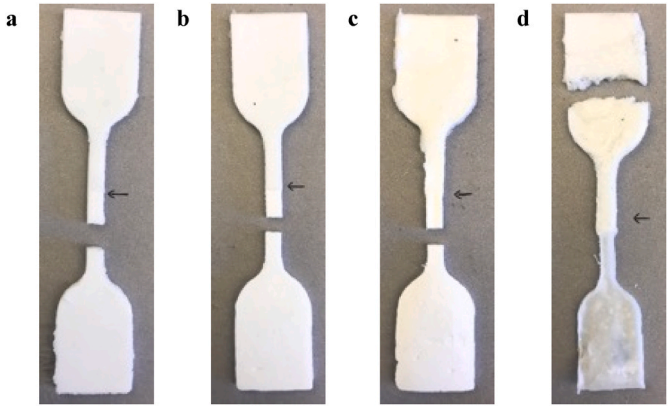

Fig. 5. Elongation at break results showing the fracture point of LP-polyHIPEs (a) LP-40/60, (b) LP-40/70, (c) LP-40/75), and (d) LP-40/80. The black arrow in each image shows the interface between two different formulations.

LP-polyHIPEs possessed values of G′ between ~80 and 140 kPa.

The polyHIPEs were further characterized using tensile testing (Fig. S6), where tension was applied in the direction normal to the interface (as opposed to the dynamic mechanical analysis experiments), and the recorded Young's Moduli (E), Ultimate Tensile Strength (σ_{ult}), and Fracture Strain (ε_f) are listed in Table 3.

As expected, the total porosity had a significant impact on the Young's moduli for the SP-polyHIPEs, where polyHIPE SP-40 and SP-80 with the lowest porosity possess the highest moduli of 96 kPa and 218 kPa respectively. The remaining polyHIPEs SP-60, SP-70, and SP-75 all obtained similar values of E of approximately 70 kPa as they all have similar total porosity values. Similar trends were observed in both the ultimate tensile strength (σ_{ult}) and fracture strain (ε_f). PolyHIPEs SP-60, SP-70, and SP-75, having comparable porosity values, all obtained values of σ_{ult} and ε_f of approximately 60 kPa and 80% respectively. PolyHIPE SP-40 had the lowest values for both σ_{ult} and ε_f of 26 kPa and 28% respectively. As this material is mostly crosslinked bulk PDMS, it was expected to have a low fracture strain compared to more porous materials theoretically [63]. PolyHIPE SP-80, having the lowest porosity, obtained the highest σ_{ult} of 150 kPa. Interestingly, this material also showed a high ε_f of 78%. We hypothesize this is possibly due to the remaining microporous porous structure after the drying process allowing the material to remain ductile. Piszczyk and coworkers [64] showed the introduction of microporosity into porous poly(urethane)s showed a similar increase in the fracture strain. Importantly, when the LP-polyHIPEs were examined by tensile testing we do not see any significant decrease in the value of E, σ_{ult}, or ε_f even though we were pulling on either side of the interface in the material. In fact, we observed an increased or maintained Young's moduli confirming that the interface between the two different porosity values was strong and did not split. To further support these observations, we monitored the fracture point of each LP-polyHIPE after elongation at break experiments (Fig. 5) and found LP-polyHIPEs consistently broke on the side of the interface with the highest total porosity. For example, polyHIPE LP-40/75 (Fig. 5c), shows a fracture point ~3 mm away from the interface on the side with a higher porosity. We observed material failure on the side from the 40% porosity in LP-40/80. This result again demonstrates that total porosity is dictating the strength of the material. While layered materials designed to have a side with a Φ_{theo} of 80% experienced pore collapse, the side consisting of a Φ_{theo} of 40% was ultimately the more porous side and weaker.

In order to demonstrate that we can prepare layered materials with more than two porosities, we prepared multilayer porosity polyHIPEs where we increased the number of different layers up to five, an example of this is shown in (Fig. 6).

These materials were produced from patterning emulsions in custom-built molds with five sections. For example, we patterned emulsions with 60%, 70%, and 75% volume of dispersed phases in the order 75% – 70% – 60% – 70% – 75% where the emulsion with 70% volume dispersed phase is dyed blue (Fig. 6a). We imaged the patterned emulsions before (Fig. 6a) and after (Fig. 6b) polymerization and found that defined interfaces were qualitatively observed between each emulsion and no inter-layer mixing occurred. These materials demonstrate that the methods described here can make multilayered polyHIPEs, we expect that the properties of the multilayered materials will be reflective of the individual SP-polyHIPEs used to prepare them. We

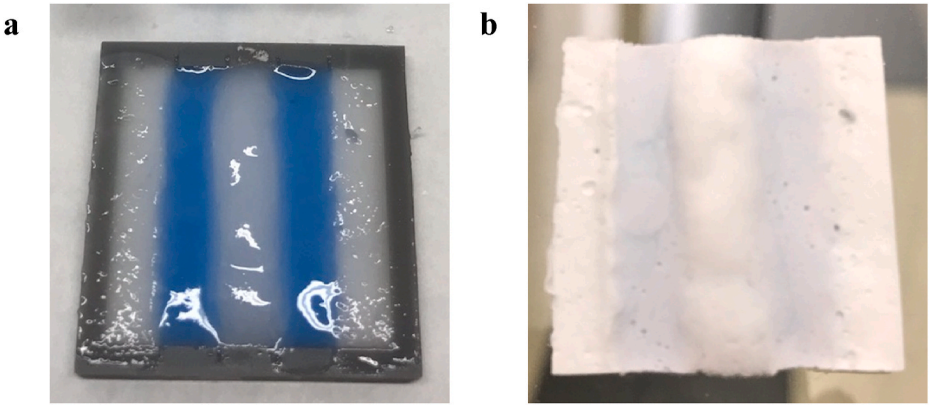

Fig. 6. Optical images of (**a**) patterned HIPEs and (**b**) multilayer polyHIPE after polymerization consisting of 75% (**outer left and right**), 70% (**center left and right**), and 60% (**middle**) volumes of dispersed phase. The 70% volume of dispersed phase emulsion was dyed blue to show the interface between different formulations. (For interpretation of the references to colour in this figure legend, the reader is referred to the Web version of this article.)

anticipate that these materials may be applicable to areas including tissue engineering scaffolds and we will report their full characterization in future publications.

4. Conclusions

We have prepared layered porosity PDMS polyHIPEs using photo-initiated thiol-ene polymerization coupled with simple emulsion patterning techniques. The volume of the dispersed phased in the emulsion dictates the total porosity and average pore size in a predictable fashion and different desired pore sizes can be imparted into a single monolith with a defined interface by selectively patterning differing emulsion formulations. The portion of the material containing the interface obtains viscoelastic characteristic representative of a blend of both compositions when tension is applied along the interface. Layered porosity polyHIPEs showed mechanically strong interfaces in tensile testing experiments, where the material fails on the softer, more porous portion rather than at the interface when tension is applied normal to the direction of the interface. This templating technique can be used to produce polyHIPEs with up to five patterned emulsions where the interface between each formulation is clear. These results prove the rapid thiol-ene polymerization occurs between each layer without disrupting the desired porous nature producing mechanically robust layered porosity materials.

CRediT authorship contribution statement

Tucker J. McKenzie: Methodology, Investigation, Writing – original draft, Visualization. **Soren Smail:** Investigation. **Kathryn Rost:** Investigation. **Kabir Rishi:** Investigation, Formal analysis, Writing – original draft. **Gregory Beaucage:** Supervision. **Neil Ayres:** Conceptualization, Writing – original draft, Writing – review & editing, Supervision, Project administration, Funding acquisition.

Declaration of competing interest

The authors declare that they have no known competing financial interests or personal relationships that could have appeared to influence the work reported in this paper.

Acknowledgements

TJM, SS, KR, and NA thank the National Science Foundation (DMR-1940518) for the resources to conduct this work, and thank Hope Kumakli, Spencer Hendrickson, Prof. Robert Lazenby, and Prof. Ryan White for help with optical microscopy images and 3D printing of the templates used in this work. KR and GB acknowledge use of the resources of the Advanced Photon Source (APS), a U.S. Department of Energy Office of Science User Facility operated for the DOE Office of Science by Argonne National Laboratory under Contract no. DE-AC02-06CH11357. The USAXS data were collected at the APS on the beamline 9-ID-C. K.R. and G.B. also acknowledge the assistance of Jan Ilavsky and Ivan Kuzmenko at Argonne National Laboratory for their help during the X-ray scattering measurements.

Appendix A. Supplementary data

Supplementary data to this article can be found online at https://doi.org/10.1016/j.polymer.2021.124116.

References

[1] G. Tang, H. Zhang, Y. Zhao, Y. Zhang, X. Li, X. Yuan, Preparation of PLGA scaffolds with graded pores by using a gelatin-microsphere template as porogen, J. Biomater. Sci. Polym. Ed. 23 (2012) 2241–2257, https://doi.org/10.1163/156856211X614185.

[2] B.A. Dikici, S. Dikici, G.C. Reilly, S. MacNeil, F. Claeyssens, A novel bilayer polycaprolactone membrane for guided bone regeneration: combining electrospinning and emulsion templating, Materials 12 (2019) 2643, https://doi.org/10.3390/ma12162643.

[3] A.P. Kishan, A.B. Robbins, S.F. Mohiuddin, M. Jiang, M.R. Moreno, E.M. Cosgriff-Hernandez, Fabrication of macromolecular gradients in aligned fiber scaffolds using a combination of in-line blending and air-gap electrospinning, Acta Biomater. 56 (2017) 118–128, https://doi.org/10.1016/j.actbio.2016.12.041.

[4] U. D'Amora, M. D'Este, D. Eglin, F. Safari, C.M. Sprecher, A. Gloria, R. De Santis, M. Alini, L. Ambrosio, Collagen density gradient on three-dimensional printed poly (ε-caprolactone) scaffolds for interface tissue engineering, J. Tissue Eng. Regen. Med. 12 (2018) 321–329, https://doi.org/10.1002/term.2457.

[5] N. Sears, P. Dhavalikar, M. Whitely, E. Cosgriff-Hernandez, Fabrication of biomimetic bone grafts with multi-material 3D printing, Biofabrication 9 (2017), 025020, https://doi.org/10.1088/1758-5090/aa7077.

[6] Z. Ma, J. Lin, X. Xu, Z. Ma, L. Tang, C. Sun, D. Li, C. Liu, Y. Zhong, L. Wang, Design and 3D printing of adjustable modulus porous structures for customized diabetic foot insoles, Int. J. Light Mater. Manuf. 2 (2019) 57–63, https://doi.org/10.1016/j.ijlmm.2018.10.003.

[7] G.V. Salmoria, C.H. Ahrens, P. Klauss, R.A. Paggi, R.G. Oliveira, A. Lago, Rapid manufacturing of polyethylene parts with controlled pore size gradients using selective laser sintering, Mater. Res. 10 (2007) 211–214, https://doi.org/10.1590/S1516-14392007000200019.

[8] S.C. Hess, A.X. Kohll, R.A. Raso, C.M. Schumacher, R.N. Grass, W.J. Stark, Template-particle stabilized bicontinuous emulsion yielding controlled assembly of hierarchical high-flux filtration membranes, ACS Appl. Mater. Interfaces 7 (2015) 611–617, https://doi.org/10.1021/am506737n.

[9] R. Kumar, Y. Jin, S. Marre, O. Poncelet, T. Brunet, J. Leng, O. Mondain-Monval, Drying kinetics and acoustic properties of soft porous polymer materials, J. Porous Mater. 28 (2020) 249–259, https://doi.org/10.1007/s10934-020-00987-w.

[10] A. Kovalenko, K. Zimny, B. Mascaro, T. Brunet, O. Mondain-Monval, Tailoring of the porous structure of soft emulsion-templated polymer materials, Soft Matter 12 (2016) 5154–5163, https://doi.org/10.1039/C6SM00461J.

[11] B. Kieback, A. Neubrand, H. Riedel, Processing techniques for functionally graded materials, Mater. Sci. Eng. 362 (2003) 81–106, https://doi.org/10.1016/S0921-5093(03)00578-1.

[12] A. Seidi, M. Ramalingam, I. Elloumi-Hannachi, S. Ostrovidov, A. Khademhosseini, Gradient biomaterials for soft-to-hard interface tissue engineering, Acta Biomater. 7 (2011) 1441–1451, https://doi.org/10.1016/j.actbio.2011.01.011.

[13] M.T. Frassica, C.J. Demott, E.M. Ramirez, M.A. Grunlan, Spatially controlled templated hydrogels for orthopedic interfacial tissue regeneration, ACS Macro Lett. 9 (2020) 1740–1744, https://doi.org/10.1021/acsmacrolett.0c00712.

[14] R. Scaffaro, F. Lopresti, L. Botta, S. Rigogliuso, G. Ghersi, Integration of PCL and PLA in a monolithic porous scaffold for interface tissue engineering, J. Mech. Behav. Biomed. Mater. 63 (2016) 303–313, https://doi.org/10.1016/j.jmbbm.2016.06.021.

[15] R. Scaffaro, F. Lopresti, L. Botta, S. Rigogliuso, G. Ghersi, Preparation of three-layered porous PLA/PEG scaffold: relationship between morphology, mechanical behavior and cell permeability, J. Mech. Behav. Biomed. Mater. 54 (2016) 8–20, https://doi.org/10.1016/j.jmbbm.2015.08.033.

[16] B. Koohbor, A. Kidane, Design optimization of continuously and discretely graded foam materials for efficient energy absorption, Mater. Des. 102 (2016) 151–161, https://doi.org/10.1016/j.matdes.2016.04.031.

[17] S. Andrieux, W. Drenckhan, C. Stubenrauch, Highly ordered biobased scaffolds: from liquid to solid foams, Polymer 126 (2017) 425–431, https://doi.org/10.1016/j.polymer.2017.04.031.

[18] B.A. Dikici, F. Claeyssens, Basic principles of emulsion templating and its use as an emerging manufacturing method of tissue engineering scaffolds, Front. Bioeng. Biotechnol. 8 (2020) 875, https://doi.org/10.3389/fbioe.2020.00875.

[19] M.S. Silverstein, PolyHIPEs: recent advances in emulsion-templated porous polymers, Prog. Polym. Sci. 38 (2014) 199–234, https://doi.org/10.1016/j.progpolymsci.2013.07.003.

[20] I. Pulko, P. Krajnc, High internal phase emulsion templating - a path to hierarchically porous functional polymers, Macromol. Rapid Commun. 33 (2012) 1731–1746, https://doi.org/10.1002/marc.201200393.

[21] S.D. Kimmins, N.R. Cameron, Functional porous polymers by emulsion templating: recent advances, Adv. Funct. Mater. 21 (2011) 211–225, https://doi.org/10.1002/adfm.201001330.

[22] N. Brun, S. Ungureanu, H. Deleuze, R. Backov, Hybrid foams, colloids and beyond: from design to applications, Chem. Soc. Rev. 40 (2011) 771–788, https://doi.org/10.1039/b920518g.

[23] I. Pulko, P. Krajnc, Porous polymer monoliths by emulsion templating, Encycl. Polym. Sci. Technol (2017) 1–28, https://doi.org/10.1002/0471440264.pst653.

[24] A. Ajdari, S. Babaee, A. Vaziri, Mechanical properties and energy absorption of heterogeneous and functionally graded cellular structures, Procedia Eng. 10 (2011) 219–223, https://doi.org/10.1016/j.proeng.2011.04.039.

[25] C. Stubenrauch, A. Menner, A. Bismarck, W. Drenckhan, Emulsion and foam templating—promising routes to Tailor-made porous polymers, Angew. Chem. Int. Ed. 57 (2018) 10024–10032, https://doi.org/10.1002/anie.201801466.

[26] R. Wu, A. Menner, A. Bismarck, Macroporous polymers made from medium internal phase emulsion templates: effect of emulsion formulation on the pore structure of polyMIPEs, Polymer 54 (2013) 5511–5517, https://doi.org/10.1016/j.polymer.2013.08.029.

[27] S. Jurjevec, E. Žagar, S. Kovačič, Functional macroporous amphoteric polyelectrolyte monoliths with tunable structures and properties through

emulsion-templated synthesis, J. Colloid Interface Sci. 575 (2020) 480–488, https://doi.org/10.1016/j.jcis.2020.05.016.
[28] W.C.E. Schofield, C.D. Bain, J.P.S. Badyal, Cyclodextrin-functionalized hierarchical porous architectures for high-throughput capture and release of organic pollutants from wastewater, Chem. Mater. 24 (2012) 1645–1653, https://doi.org/10.1021/cm300552k.
[29] T. Watanabe, C.G. Lopez, J.F. Douglas, T. Ono, J.T. Cabral, Microfluidic approach to the formation of internally porous polymer particles by solvent extraction, Langmuir 30 (2014) 2470–2479, https://doi.org/10.1021/la404506b.
[30] J. Elsing, A. Quell, C. Stubenrauch, Toward functionally graded polymer foams using microfluidics, Adv. Eng. Mater. 19 (2017) 1–5, https://doi.org/10.1002/adem.201700195.
[31] C.R. Langford, D.W. Johnson, N.R. Cameron, Preparation of hybrid thiol-acrylate emulsion-templated porous polymers by interfacial copolymerization of high internal phase emulsions, Macromol. Rapid Commun. 36 (2015) 834–839, https://doi.org/10.1002/marc.201400733.
[32] M. Sušec, S.C. Ligon, J. Stampfl, R. Liska, P. Krajnc, Hierarchically porous materials from layer-by-layer photopolymerization of high internal phase emulsions, Macromol. Rapid Commun. 34 (2013) 938–943, https://doi.org/10.1002/marc.201300016.
[33] S. Xie, F. Svec, J.M.J. Fréchet, Preparation of porous hydrophilic monoliths: effect of the polymerization conditions on the porous properties of poly (acrylamide-co-N,N′-methylenebisacrylamide) monolithic rods, J. Polym. Sci. Part A Polym. Chem. 35 (1997) 1013–1021, https://doi.org/10.1002/(sici)1099-0518(19970430)35:6<1013::aid-pola4>3.3.co;2-7.
[34] S. Kovačič, N. Drašinac, A. Pintar, E. Žagar, Highly porous cationic polyelectrolytes via oil-in-water concentrated emulsions: synthesis and adsorption kinetic study, Langmuir 34 (2018) 10353–10362, https://doi.org/10.1021/acs.langmuir.8b01645.
[35] N.R. Cameron, A. Barbetta, The influence of porogen type on the porosity, surface area and morphology of poly(divinylbenzene) polyHIPE foams, J. Mater. Chem. 10 (2000) 2466–2471, https://doi.org/10.1039/B003596N.
[36] R.J. Carnachan, M. Bokhari, S.A. Przyborski, N.R. Cameron, Tailoring the morphology of emulsion-templated porous polymers, Soft Matter 2 (2006) 608–616, https://doi.org/10.1039/b603211g.
[37] J.S. Lim, S.F. Wong, M.C. Law, Y. Samyudia, S.S. Dol, A review on the effects of emulsions on flow behaviours and common factors affecting the stability of emulsions, J. Appl. Sci. 15 (2015) 167–172, https://doi.org/10.3923/jas.2015.167.172.
[38] P. Steindl, H. Decker, B. Retzl, Q. Jiang, A. Menner, A. Bismarck, Emulsion-templated flexible epoxy foams, Polymer 215 (2021) 123380, https://doi.org/10.1016/j.polymer.2021.123380.
[39] H.C. Kolb, M.G. Finn, K.B. Sharpless, Click chemistry: diverse chemical function from a few good reactions, Angew. Chem. Int. Ed. 40 (2001) 2–5, https://doi.org/10.1002/1521-3773(20010601)40:11<2004::AID-ANIE2004>3.0.CO, 2004–2021.
[40] R.K. Iha, K.L. Wooley, A.M. Nyström, D.J. Burke, M.J. Kade, C.J. Hawker, Applications of orthogonal "click" chemistries in the synthesis of functional soft materials, Chem. Rev. 109 (2009) 5620–5686, https://doi.org/10.1021/cr900138t.
[41] M.J. Kade, D.J. Burke, C.J. Hawker, The power of thiol-ene chemistry, J. Polym. Sci. Part A Polym. Chem. 48 (2010) 743–750, https://doi.org/10.1002/pola.23824.
[42] C.E. Hoyle, C.N. Bowman, Thiol-ene click chemistry, Angew. Chem. Int. Ed. 49 (2010) 1540–1573, https://doi.org/10.1002/anie.200903924.
[43] A.B. Lowe, Thiol-ene "click" reactions and recent applications in polymer and materials synthesis: a first update, Polym. Chem. 5 (2014) 4820–4870, https://doi.org/10.1039/c4py00339j.
[44] E. Lovelady, S.D. Kimmins, J. Wu, N.R. Cameron, Preparation of emulsion-templated porous polymers using thiol-ene and thiol-yne chemistry, Polym. Chem. 3 (2011) 559–562, https://doi.org/10.1039/c0py00374c.
[45] M. Sušec, R. Liska, G. Russmüller, J. Kotek, P. Krajnc, Microcellular open porous monoliths for cell growth by thiol-ene polymerization of low-toxicity monomers in high internal phase emulsions, Macromol. Biosci. 15 (2015) 253–261, https://doi.org/10.1002/mabi.201400219.
[46] D.W. Johnson, C.R. Langford, M.P. Didsbury, B. Lipp, S.A. Przyborski, N. R. Cameron, Fully biodegradable and biocompatible emulsion templated polymer scaffolds by thiol-acrylate polymerization of polycaprolactone macromonomers, Polym. Chem. 6 (2015) 7256–7263, https://doi.org/10.1039/c5py00721f.
[47] P. Shen, S.Z. Moghaddam, Q. Huang, A.E. Daugaard, S. Zhang, P. Szabo, Hard-soft thiol-ene materials without interfacial weakness, Mater. Today Commun. 21 (2019) 100657, https://doi.org/10.1016/j.mtcomm.2019.100657.
[48] T. Kobayashi, H. Saitoh, N. Fujii, Y. Hoshino, M. Takanashi, Porous membrane of polydimethylsiloxane by hydrosilylation cure: characteristics of membranes having pores formed by hydrogen foams, J. Appl. Polym. Sci. 50 (1993) 971–979, https://doi.org/10.1002/app.1993.070500606.
[49] M.T. Grosse, M. Lamotte, M. Birot, H. Deleuze, Preparation of microcellular polysiloxane monoliths, J. Polym. Sci. Part A Polym. Chem. 46 (2008) 21–32, https://doi.org/10.1002/pola.22351.
[50] A. Kataruka, S.B. Hutchens, PDMS polymerized high internal phase emulsions (polyHIPEs) with closed-cell, aqueous-filled microcavities, Soft Matter 15 (2019) 9665–9675, https://doi.org/10.1039/c9sm01732a.
[51] T.J. McKenzie, P.S. Heaton, K. Rishi, R. Kumar, T. Brunet, G. Beaucage, O. Mondain-Monval, N. Ayres, Storage moduli and porosity of soft PDMS PolyMIPEs can Be controlled independently using thiol-ene click chemistry, Macromolecules 53 (2020) 3719–3727, https://doi.org/10.1021/acs.macromol.0c00217.
[52] J. Ilavsky, F. Zhang, R.N. Andrews, I. Kuzmenko, P.R. Jemian, L.E. Levine, A. J. Allen, Development of combined microstructure and structure characterization facility for in situ and operando studies at the advanced photon source, J. Appl. Crystallogr. 51 (2018) 867–882, https://doi.org/10.1107/S160057671800643X.
[53] J. Ilavsky, F. Zhang, A.J. Allen, L.E. Levine, P.R. Jemian, G.G. Long, Ultra-small-angle X-ray scattering instrument at the advanced photon source: history, recent development, and current status, Metall. Mater. Trans. A Phys. Metall. Mater. Sci. 44 (2013) 68–76, https://doi.org/10.1007/s11661-012-1431-y.
[54] J. Ilavsky, P.R. Jemian, Irena: tool suite for modeling and analysis of small-angle scattering, J. Appl. Crystallogr. 42 (2009) 347–353, https://doi.org/10.1107/S0021889809002222.
[55] N. Hu, N. Borkar, D. Kohls, D.W. Schaefer, Characterization of porous materials using combined small-angle X-ray and neutron scattering techniques, J. Membr. Sci. 379 (2011) 138–145, https://doi.org/10.1016/j.memsci.2011.05.053.
[56] G. Porod, Die Röntgenkleinwinkelstreuung von dichtgepackten kolloiden Systemen - I. Teil, Kolloid Z. 124 (1951) 83–114, https://doi.org/10.1007/BF01512792.
[57] P. Debye, H.R. Anderson, H. Brumberger, Scattering by an inhomogeneous solid. II. the correlation function and its application, J. Appl. Phys. 28 (1957) 679–683, https://doi.org/10.1063/1.1722830.
[58] J. Ilavsky, Nika: software for two-dimensional data reduction, J. Appl. Crystallogr. 45 (2012) 324–328, https://doi.org/10.1107/S0021889812004037.
[59] G. Beaucage, H.K. Kammler, S.E. Pratsinis, Particle size distributions from small-angle scattering using global scattering functions, J. Appl. Crystallogr. 37 (2004) 523–535, https://doi.org/10.1107/S0021889804008969.
[60] E. Pedraza, A.-C. Brady, C.A. Fraker, C.L. Stabler, Synthesis of macroporous poly (dimethylsiloxane) scaffolds for tissue engineering applications, J. Biomater. Sci. Polym. Ed. 24 (2013) 1041–1056, https://doi.org/10.1080/09205063.2012.735097.Synthesis.
[61] M.F. Ashby, The properties of foams and lattices, Philos. Trans. R. Soc. A Math. Phys. Eng. Sci. 364 (2006) 15–30, https://doi.org/10.1098/rsta.2005.1678.
[62] S. Peng, P.G. Hartley, T.C. Hughes, Q. Guo, Controlling morphology and porosity of porous siloxane membranes through water content of precursor microemulsion, Soft Matter 8 (2012) 10493–10501, https://doi.org/10.1039/c2sm26312b.
[63] S. Kovačič, E. Žagar, C. Slugovc, Strength versus toughness of emulsion templated Poly(Dicyclopentadiene) foams, Polymer 169 (2019) 58–65, https://doi.org/10.1016/j.polymer.2019.02.045.
[64] A. Hejna, P. Kosmela, M. Mikicka, M. Danowska, L. Piszczyk, Modification of microporous polyurethane elastomers with different types of ash—morphological, mechanical, and thermal studies, Polym. Compos. 37 (2016) 881–889, https://doi.org/10.1002/pc.